

**A Model for Moisture Transport in a
High-Level Radioactive Waste Repository Drift**

**Steve T. Green,
Southwest Research Institute®
San Antonio, Texas**

**David B. Walter
Southwest Research Institute®
San Antonio, Texas**

**Randall W. Fedors
CNWRA - Southwest Research Institute®
San Antonio, Texas**

**Franklin T. Dodge
Southwest Research Institute®
San Antonio, Texas**

(For SME Feb 2004 Annual Meeting – Hydrology Session)

ABSTRACT

Spatial and temporal temperature variations in a high-level radioactive waste repository drift can give rise to moisture transport within the drift. Knowledge of this moisture transport may be important to assessing the potential for corrosion of all metallic components in the drift. The model presented here shows one approach to simulating evaporation, transport, and condensation of water in large underground openings using a framework based on computational fluid dynamics. Simulation results that explicitly model water and latent heat transport are presented.

INTRODUCTION

A sketch of a waste container in an emplacement drift is shown in Figure 1. Temperature differences along the drift are expected to occur because waste packages may have different heat loads, rock properties may change along the drift, or the waste packages may not extend the entire length of the drift. So, it is expected that natural convection will be established between hotter zones and cooler zones in the drift. If groundwater is present at the driftwall surface, the heated air will evaporate water from the walls near the hot containers and transport it to the cooler zones where it will condense. This so-called cold-trap effect has been observed in emplacement drifts in which tunnel boring machines have heated one end of a sealed drift (Bechtel SAIC, 2001). After a period of time, some unknown portion of the standing water found at cool portions of the drift could unambiguously be attributed to the cold-trap process.

In addition to condensation, the thermally driven convection cells may act as a source for moisture returning to hot areas. During the cool down phase after peak temperatures have been reached, the wallrock will

slowly begin to rewet. The relative humidity near the waste packages will increase because of the decreasing temperature and because of the supply of moisture from the slowly rewetting wallrock. Thermally driven convection cells may provide an additional source of water from cool wet areas to hot dry areas, thus leading to elevated relative humidities much sooner than would be estimated if convection were not considered.

It is thought that the moisture redistribution and the cold-trap effect could occur along a line of containers that were not all at the same temperature. In this instance, small circulation cells between groups of waste packages may cause water to condense on cooler packages or nearby drip shields, or to locally raise the relative humidity enough so that deliquescence might lead to the presence of liquid phase water on waste packages. Regardless of the extent of the circulation cell, natural convection and the cold-trap effect are of concern because the presence of water and dissolved salts have the potential to accelerate the corrosion of drip shields and waste packages.

The cold-trap effect has been duplicated in a laboratory experiment that is roughly a 0.01 scale of an emplacement drift. The experimental and numerical simulation results are reported by Fedors, et al. (2003) and Walter et al. (2004). In those studies, the effects of evaporation and condensation were not included in the energy transport equations. Furthermore, moisture transport was estimated from a calculation that was uncoupled from the computation of mass, momentum and energy transport. Even so, it was demonstrated that the cold-trap effect could move measurable quantities of water at small temperature gradients in the scaled experiment.

The complex geometries and close coupling of the transport processes require that computational fluid dynamic (CFD) approaches be used to simulate the

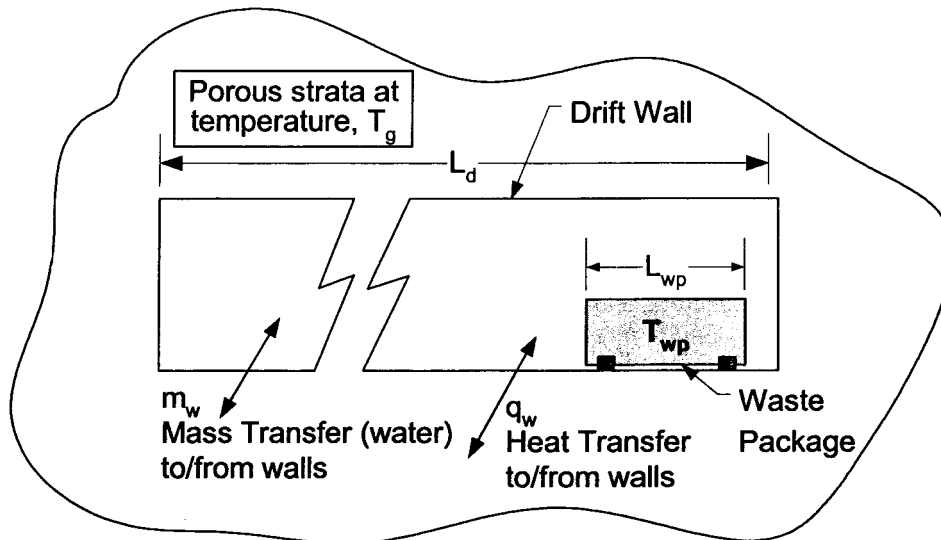


Figure 1. Schematic of a Container in an Emplacement Drift

A container at temperature T_a greater than the rock temperature T_g and placed far from the drift end will create a natural convection cell that will transport energy and moisture from the warm end to the cool end.

convection within an emplacement drift. The prominent commercial CFD codes, however, do not adequately treat evaporation and condensation of water vapor. The goal of this investigation is to develop a simple but effective algorithm for evaporation and condensation to incorporate in a model for the bulk flow and heat transfer and the moisture transport in a drift. This report describes the initial stages in the development of this model and concludes with recommendations for making the model applicable to a wide range of drift operating conditions.

MODEL DESCRIPTION

This section summarizes an evaporation/condensation model suitable for including in CFD simulations. The assumptions underlying the model are first listed. This is followed by a description of the algorithm. Example calculations are presented in the next section.

Assumptions

- The fluid is considered to be a binary mixture of water vapor and air, each of which are considered to be ideal gases. (Of course, the air is itself a mixture of many gases, but is considered here to be a single component).
- Thermo-diffusion is negligible. Advection and Fickian diffusion effects are assumed to be much greater than the Soret effect.
- The Boussinesq assumption is applied here. That is the vapor/air mixture is nominally incompressible but the density varies slightly from its mean value due to the isobaric thermal expansion coefficient.
- Liquid water is always available at the drift walls and there is no effect of the porous walls on the water saturation pressure. This restriction may be relaxed in the future to include the capillary effects of the porous drift walls.
- Temperatures are below the boiling point of the water at the mean drift pressure. Thus, evaporation/condensation is dictated solely by comparing the local water vapor partial pressure to the saturation vapor pressure of water.
- Phase change takes place only at the drift walls. In other words, condensation in the open flow field is not allowed. This simplifies the flow model in that two-phase flow (droplets in the air) is not considered. This is one of the most significant simplifying assumptions made here.
- Condensate layers are not thick enough to cause film flow on the walls. This is equivalent to the condensate being assumed to be adiabatically absorbed into the wall.
- Evaporation and condensation mass fluxes are much greater than the advection and diffusion fluxes. Vapor flow rates to or from walls are not limited. It is seen below that this is another important assumption.

Governing Equations

The governing equations for the bulk flow are those appropriate for a nominally incompressible fluid in which the fluid has a small variation in volume with temperature (i.e., the Boussinesq approximation). These equations are as follows:

Mass Conservation:

$$\nabla \cdot \vec{V} = 0 \quad (1)$$

Momentum Conservation:

$$\rho \frac{D\vec{V}}{Dt} = \mu \nabla^2 \vec{V} - \rho \mathbf{g} \quad (2)$$

Energy Conservation:

$$\frac{D\rho e}{Dt} = k \nabla^2 T + \dot{q}''''_{source} \quad (3)$$

The following definitions apply to Equations (1), (2), and (3).

- \vec{V} = fluid velocity vector
- ρ = mixture density
- \mathbf{g} = acceleration due to gravity
- μ = mixture viscosity
- k = mixture thermal conductivity
- e = mixture thermodynamic internal energy
- \dot{q}'''' = volume specific energy source
- t = time

Under the modeling assumptions described above, the principle of conservation of chemical species can be used to derive an equation for the transport of water vapor in an air/water vapor mixture [e.g., see Burmeister (1983)],

$$\rho \frac{Dc_v}{Dt} = \nabla \cdot (\rho D \nabla c_v) + \dot{m}''''_{source} \quad (4)$$

where ρ = mixture density

c_v = vapor concentration

D = binary diffusion coefficient for water vapor/air

\dot{m}''''_{source} = vapor mass flux at walls.

For turbulent flows, the concept of the eddy diffusivity is used in the time-averaged form of the conservation equations to include the effects of turbulent diffusion of momentum, energy, and molecular species. The choice of turbulence model is problem specific and is not the focus of this report.

The flow is nominally incompressible, but the density variations due to buoyancy and composition must be approximated. For single-component flows, a thermal expansion coefficient generally is defined for the fluid and the density is adjusted locally as a function of the deviation from a baseline density defined at a reference temperature. For the two-component mixture studied here, however, the combined buoyancy and composition effects on the local fluid density are computed via the expression,

$$\rho = \frac{P_a M_a + P_v M_v}{R_g T} \quad (5)$$

where ρ = mixture density

P_a = local partial pressure air

P_v = local partial pressure of water

M_a = molecular weight of air

M_v = molecular weight of water

R_g = universal gas constant

T = local temperature

Several of the commercially available CFD packages allow for the inclusion of advection/diffusion of chemical species, but the details of computing the source term \dot{m}^m in Eq. (4) are the key to providing the correct rate of generation and removal of the scalar species, which in this case is water.

Phase Change Algorithm

Consider a computational mesh unit adjacent to the wall as a control volume. The phase change at the walls is dictated by whether the water vapor partial pressure in this small volume is below the saturation water vapor pressure. In this simple model, phase change will take place so that the water vapor partial pressure in the small volume near the wall is maintained at its saturation condition. In order for the water to change phase, energy must be either supplied (during evaporation) to it or removed (during condensation) from it. That is, it is assumed that the phase change rate time scale is much smaller than the advection and diffusion time scales. The alternative is to estimate the phase change rate based on kinetic theory, experimental mass transfer data, or some other rate-based formulation.

The diffusion and advection of the air/vapor accounted for in the solution algorithm for Eq. (4) establishes the local vapor concentration at the beginning of the phase change calculation. During a single time step in the CFD computation process, the phase change process in the computational mesh cells near the wall is viewed as an idealized mixing scenario. The air and the portion of the vapor that does not undergo phase change are assumed to be fixed for the purpose of calculating the phase change rate. This fixed portion of the total mass exchanges energy with either the liquid on the wall or the condensing vapor in the volume to correspond to latent heat of the water that is either evaporated from or condensed onto the wall. The conservation of energy in this scenario is given by

$$m_1(e_2 - e_1) = h_{vap} m_w = h_{vap} [m_{v,sat} - m_{v1}]$$

where

m_1 = air/vapor mass in control volume that does not undergo the phase change

m_{v1} = vapor mass in control volume that does not under go the phase change

$m_{v,sat}$ = vapor mass in control volume after the phase change (the air is saturated after the phase change)

h_{vap} = heat of vaporization of the water

e_2 = mixture energy after the phase change

e_1 = mixture energy prior to the phase change.

This can be reduced to the following expression,

$$e_2 - e_1 = h_{vap} \left[\frac{W_{sat}(T_2) - W_1}{1 + W_1} \right] \quad (6)$$

where

W_1 = humidity ratio (before phase change)

W_{sat} = saturation humidity ratio (after phase change)

T_2 = air/vapor mixture temperature after phase change

The humidity ratio is the ratio of the vapor mass to the dry air mass. The term, $W_{sat}(T_2)$, is given in this form to highlight the fact that this is the saturation humidity ratio at the temperature conditions at the end of the time step after the phase change has taken place. Eq. (7) is solved iteratively for the temperature, T_2 . The humidity ratio, W_1 , is determined from the known local concentration resulting from the CFD solution scheme,

$$W_1 = \frac{c_{v1}}{1 - c_{v1}}$$

where c_{v1} is the vapor concentration before the phase change is accounted for. The saturation humidity ratio is computed from the standard psychrometric relation

$$W_{sat} = \frac{P_{v,sat}}{P_{tot} - P_{v,sat}} \frac{M_v}{M_a} \quad (7)$$

It is assumed here that the saturation partial pressure of water vapor in air is the same as its saturation vapor in a simple water vapor/liquid system. The Keenan, Keyes, Hill, and Moore Formula (1969) is used to estimate the saturation vapor pressure of water vapor.

$$\ln\left(\frac{P_{v,sat}}{217.99}\right) = \frac{0.01}{T} (374.136 - t) \times \left[-741.9242 + \sum_{i=1}^7 F_i (0.65 - 0.01t)^i \right] \quad (8)$$

where

$$F_1 = -29.721$$

$$F_2 = -11.55286$$

$$F_3 = -0.8685635$$

$$F_4 = +0.1094098$$

$$T = \text{absolute temperature, Kelvin}$$

$$t = \text{temperature, } ^\circ\text{C} = T - 273.15$$

$$P_{v,sat} = \text{saturation pressure, atm}$$

$$F_5 = +0.439993$$

$$F_6 = +0.2520658$$

$$F_7 = +0.05218684$$

It should be noted that Eq. (8) is valid over the temperature range 0°C to 374°C.

Equations (6), (7), and (8) are solved iteratively to find a value of T_2 that satisfies the energy balance. Finally, the volume specific mass source term in Eq. (4) and the energy source term in Equation (3) can now be determined from

$$\dot{m}''_{source} = \rho(c_{v,sat} - c_{v1}) \quad (9)$$

$$\dot{q}''_{source} = \rho(e_2 - e_1) \quad (10)$$

For locations in the flow domain at locations other than at the walls, the vapor mass source terms and phase change energy source terms are neglected.

EXAMPLE CALCULATIONS

The model described above is being developed for use in simulating the energy and mass transport process in the complex flow fields in emplacement drifts. Before proceeding with these complicated simulations, the model described above was applied to simple examples to assess its usefulness and accuracy.

The CFD code, Flow-3D®, was modified as necessary to incorporate the phase change algorithm and the mixture property definitions described above. This was accomplished completely within the user-accessible subroutines supplied with the program.

Boundary Layer

The first example case is a simple laminar boundary layer flow. Consider the low-speed flow of dry air over a flat surface of water, Figure 2.

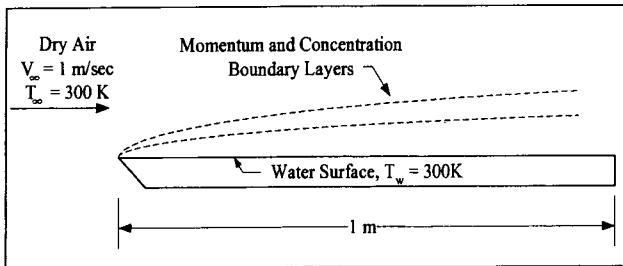


Figure 2. Boundary Layer Flow over a Water Surface
This is a classical laminar flow in which a momentum and concentration boundary layer grow into the freestream.

The Reynolds Number for this flow is approximately 6×10^4 , which indicates that the flow is laminar over the entire length of the plate. According to laminar boundary layer theory (Incropera and DeWitt, 2002), the mass transfer rate along the length of the plate can be computed from the following equations,

$$Sh_x = 0.332 Re_x^{0.5} Sc^{0.333} \quad (11)$$

where

$$Sh_x = \text{local Sherwood Number} = h_m x / D_{AB}$$

$$Re_x = \text{local Reynolds Number} = V_\infty x / \nu_\infty$$

$$x = \text{distance from leading edge}$$

V_∞ = freestream velocity

h_m = mass transfer coefficient

D_{AB} = diffusion coefficient for water-air mixture

ν_∞ = kinematic viscosity of freestream air

Sc = Schmidt Number = ν_∞ / D_{AB}

The average mass flux over the entire plate length is given by,

$$Sh_L = 0.664 Re_L^{0.5} Sc^{0.333} \quad (12)$$

where the length scale, x , is replaced by the total length of the plate, $L = 1$ m, in the variable definitions.

The mass flux is then given by

$$\dot{m}''_v = h_m (\rho_{vs} - \rho_{v\infty}) \quad (13)$$

where ρ_{vs} and $\rho_{v\infty}$ are the water vapor bulk density at the water surface and in the freestream, respectively. The air is assumed to be saturated just above the water surface, while the freestream water vapor density is $\rho_{v\infty} = 0$ in accordance with the given conditions.

For the CFD calculations, the flow field above the plate was discretized with 20 cells along the plate and 50 cells extending a distance 5 cm above the plate. The grid was uniform along the plate but a variable grid above the plate was defined with a smooth expansion from a cell height of 4×10^{-4} m.

The CFD code estimates for mass flux are compared to the laminar boundary layer theory in Figure 3. There is excellent agreement except for a short region near the leading edge. A comparison of the Sherwood Number values is provided in Figure 4. Again, there is very good agreement except close to the leading edge. This is not surprising, given the relative coarseness of the grid with respect to boundary layer thickness in this region.

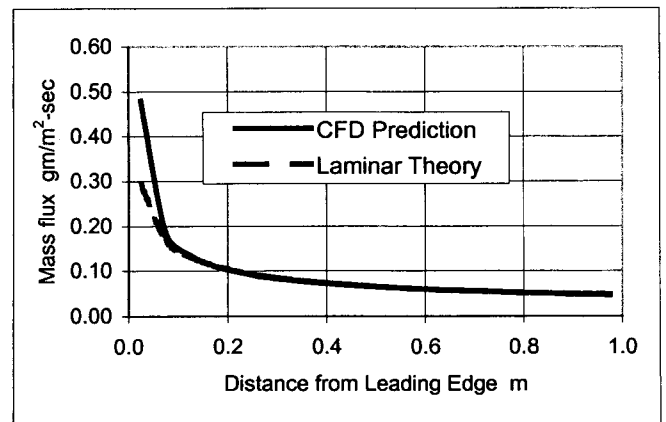


Figure 3. Evaporation Rate in Example Boundary Layer Flow. The FLOW-3D® predictions for isothermal mass flux from a flat plate agree well with laminar boundary layer theory.

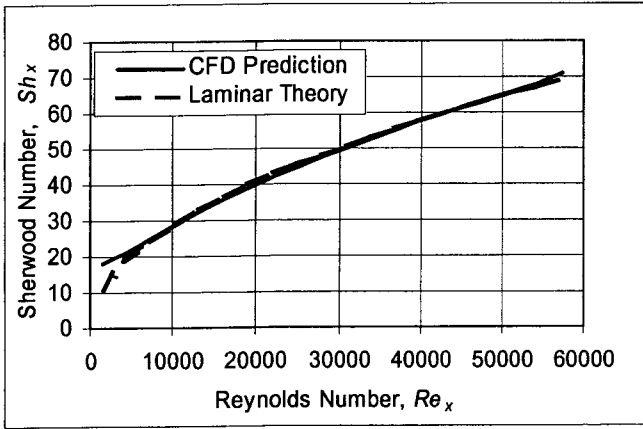


Figure 4. Sherwood Number for Flat Plate Flow
The FLOW-3D® predictions for isothermal mass flux from a flat plate agree well with laminar boundary layer theory.

Catton (1978) suggests a correlation for estimating the Nusselt Number for this condition,

$$Nu = 0.18 \left(\frac{Pr}{0.2 + Pr} Ra \right)^{0.29} \quad (14)$$

The Prandtl Number, $Pr \approx 0.72$, for this mixture. The Rayleigh Number is defined as

$$Ra = \frac{g\beta\Delta TL^3}{\alpha\nu} \quad (15)$$

- where g = gravitational acceleration
- β = thermal expansion coefficient $\approx 1/T$
- α = thermal diffusivity = $2.41 \times 10^{-5} \text{ m}^2/\text{sec}$
- ν = kinematic viscosity = $1.749 \times 10^{-5} \text{ m}^2/\text{sec}$
- ΔT = temperature difference = 40 K
- L = length scale (length of enclosure side) = 0.2 m

Natural Convection in a Square Enclosure

The second example case is a buoyancy-driven flow in a 2-D square enclosure, Figure 5. The flow domain was discretized with a 40x40 uniform grid.

The CFD steady state estimate of the velocity vectors and fluid temperatures is shown in Figure 6. A similar image for the vapor concentration contours is shown in Figure 7. These images show the expected result of a clockwise rotation in which the temperature and humidity increase as the flow goes up the hot wall. The reverse trend occurs as the flow goes down the cold wall. The net heat transfer rate for this flow is 21.6 W and the net mass transfer rate is $8.77 \times 10^{-5} \text{ kg/sec}$. These correspond to a Nusselt Number of $Nu=19.3$, and a Sherwood Number of $Sh=32.0$.

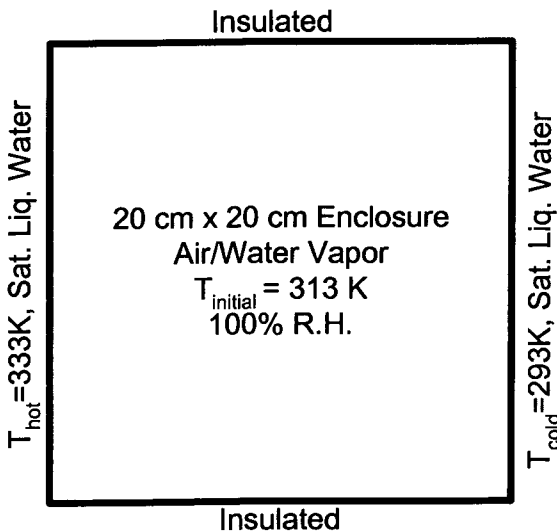
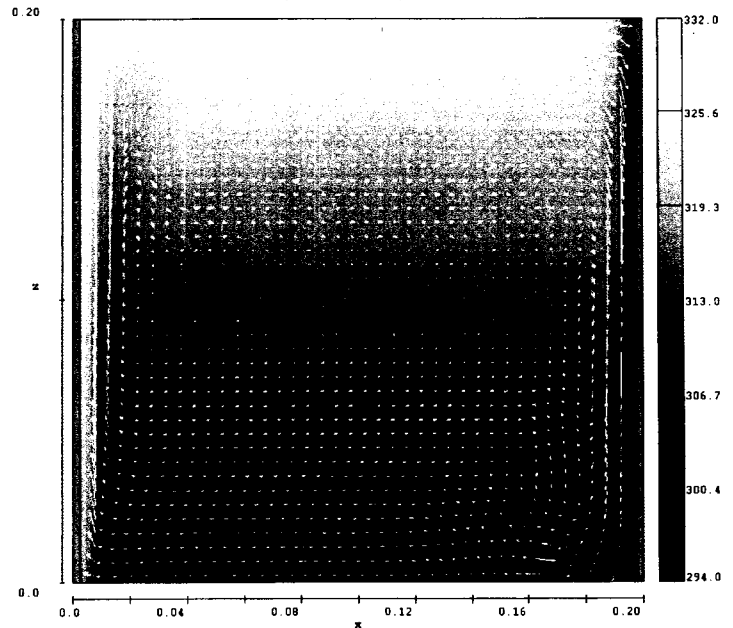
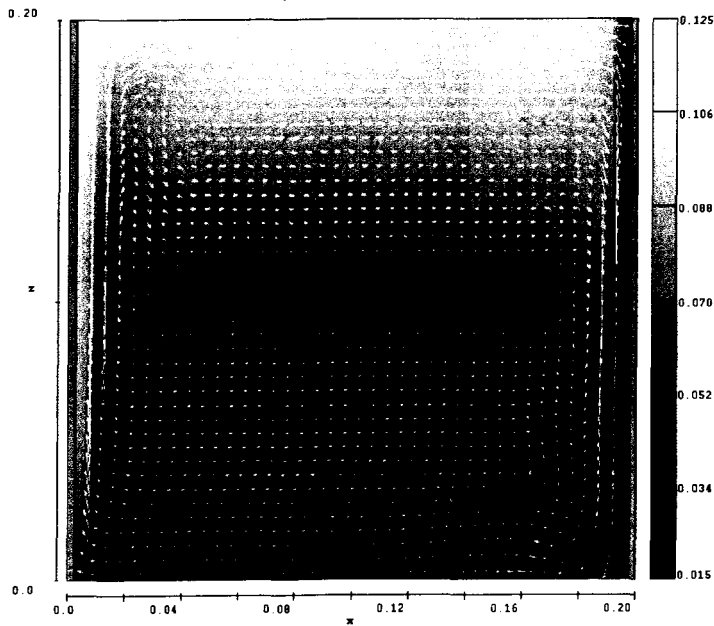


Figure 5. Natural Convection in a Square Enclosure. The gas mixture is forced into a clockwise rotation by buoyancy forces. A net flow of water across the enclosure occurs by evaporation at the hot wall and condensation at the cold wall.



FLOW-3D t=50.00 y=5.000E-01 (ix=2 to 41 kz=2 to 41)
16:31:41 10/09/2003 habq hydr3d: version 0.1.1 win32-cvf 2002

Figure 6. Predicted Temperature Field for Natural Convection Flow. The temperature contours are in Kelvins and the velocity vectors are shown by the arrows. The extreme temperatures are within 1 K of the respective wall temperatures.



FLOW-3D t=50.00 y=5.000E-01 (ix=2 to 41 kz=2 to 41)
16:31:41 10/09/2003 habq hydr3d: version 9.1.1 win32-cvf 2002

Figure 7. Predicted Vapor Concentration for Natural Convection Flow. *These vapor concentration contours are in mass fraction and the velocity vectors are shown by the arrows. There is a net mass flow of water from the hot surface to the cold caused by the rotating fluid.*

Using this correlation, the Nusselt Number is computed to be $Nu=23$. This value is about 16% greater than that provided by the CFD simulation.

Incropera and DeWitt (2002) show that, based on the analogy between mass and heat transfer, the Sherwood Number for natural convection flows can be estimated as

$$Sh = Nu \left(\frac{\alpha}{D_{AB}} \right)^{\frac{1}{3}} \quad (14)$$

The diffusion coefficient for this condition is approximately $D_{AB} = 2.6 \times 10^{-5} \text{ m}^2/\text{sec}$. So, the Sherwood Number is approximately $Sh=22.4$; about 30% less than the value predicted by CFD.

The agreement between the CFD predictions and the empirical correlations for heat and mass transfer in this case are not as close as in the classical laminar boundary case. Considering the complexity of the flow field and the uncertainty in the typical empirical correlation, this is still considered to be good agreement.

CONCLUSIONS

A simple algorithm for computing the evaporation and condensation rates between a gas mixture and a wall saturated with the liquid phase of one of the mixture constituents has been described. The phase change model was added to the commercial code, Flow-3D[®] and was

tested by comparing the model predictions of the mass transfer rates to theoretical and empirical correlations for two different flow scenarios.

The CFD model results for mass transfer rate are in close agreement with the theoretical predictions for a simple 2-D boundary layer flow. In the case of natural convection in a square enclosure, the CFD model was within 25% of an accepted empirical correlation.

These examples demonstrate the success of incorporating a complete moist air model into an available commercial CFD code. Additional testing of the model is ongoing in preparation for its use in simulations of flow patterns in thermally perturbed emplacement drifts.

A drawback to the model approach described here is that the water vapor concentration is assumed to be low enough that psychrometric equations are applicable. Emplacement drifts, however, could operate at temperature well above the normal boiling point of water in which the water vapor can completely displace the air in some portions of the drift. Approaches are currently being considered for expanding this model to allow for simulation of this multi-component, multi-phase flow field at elevated temperatures.

ACKNOWLEDGMENTS

This paper was prepared to document work performed by the Center for Nuclear Waste Regulatory Analyses (CNWRA) for the Nuclear Regulatory Commission (NRC) under Contract No. NRC-02-02-012. The activities reported here were performed on behalf of the NRC Office of Nuclear Material Safety and Safeguards, Division of Waste Management. This paper is an independent product of the CNWRA and does not necessarily reflect the view or regulatory position of the NRC.

REFERENCES

- Bechtel SAIC Company, LLC. 2001. "FY01 Supplemental Science and Performance Assessment." Vol. 1: Scientific Bases and Analyses. TDR-MGR-MD-000007. Rev. 00 ICN 01. Las Vegas, Nevada: Bechtel SAIC Company, LLC.
- Burmeister, Louis C., 1983, Convective Heat Transfer, John Wiley and Sons, New York, City, New York.
- Catton, I., 1978, "Natural Convection in Enclosures," Proceedings of the 6th International Conference, Toronto, Canada, Volume 6, p.13, Hemisphere Publishing Corp.
- Fedors, R.W., Walter, D.B., Dodge, F.T., Green, S.T., Prikryl, J.D., Svedeman, S.J., 2003, "Laboratory and Numerical Modeling of the Cold-Trap Process," CNWRA

Report, San Antonio, Texas: Center for Nuclear Waste Regulatory Analyses.

Flow Science, Inc., 2003, "FLOW-3D User's Manual." Version 8.1.1. Sante Fe, New Mexico: Flow Science, Inc.

Incropera, F.P. and D.P DeWitt. 2002. Fundamentals of Heat and Mass Transfer. John Wiley and Sons, New York City, New York.

Keenan, J. H., Keyes, F. G., Hill, P. G., Moore, J. G., 1969, Steam Tables: Thermodynamic Properties of Water, Including Vapor, Liquid, and Solid Phases, John Wiley and Sons, Inc., New York.

Walter, D.B., Green, S.T., Fedors, R.W., Hart, R. A., 2004, "Modeling a Small Laboratory Cold-Trap Experiment," Society for Mining, Metallurgy, and Exploration Annual Meeting, February 23-35, 2004, Denver, Colorado.